Construction and Building Materials 314 (2022) 125708

Contents lists available at ScienceDirect

Construction and Building Materials

journal homepage: www.elsevier.com/locate/conbuildmat

Comparison of the effects and efficiency of vertical and side tamping methods for ballasted railway tracks

Michał Przybyłowicz [a], Mykola Sysyn [a], Ulf Gerber [a], Vitalii Kovalchuk [b], Szabolcs Fischer [c,*]

[a] Institute of Railway Systems and Public Transport, Technical University of Dresden, D-01069 Dresden, Hettnerstraße 2, Germany
[b] Department of the Rolling Stock and Track, Lviv Branch of Dnipro National University of Railway Transport, UA-79052 Lviv, Ivanny Blazhkevych 12a, Ukraine
[c] Department of Transport Infrastructure and Water Resources Engineering, Faculty of Architecture, Civil- and Transport Engineering, Szechenyi Istvan University, Egyetem ter 1, Gyor 9026, Hungary

ARTICLE INFO

Keywords:
Railway ballast
Tamping technologies
Scaled modeling
Experimental measurements
Ballast compaction
Wave time of flight
Discrete element modeling

ABSTRACT

The relatively high maintenance costs of the ballast track are related to the short lifecycle of the ballast layer. The current vertical ballast tamping technology (e.g., Plasser & Theurer, Matisa, etc.) causes high ballast destruction and is neither applicable for unconventional sleepers' designs nor slab tracks. The side tamping method presents an alternative, ballast saving, and sleeper form independent ballast tamping technology. This paper compares the ballast layer compaction and its resistance to permanent settlements accumulation after the vertical and the side tamping methodologies. Scaled models of ballast layer and tamping units and scaled simulation with discrete element method (DEM) were applied for the comparison. In the laboratory tests, the ballast compaction along the sleeper was estimated using the measurements of elastic wave propagation. The settlements resistance for both tamping methods was estimated under the vibration loading. The tests' results show 5–7% higher compactness of the ballast layer under the sleeper ends for the side tamping method. The settlement intensity of the ballast layer after the vertical tamping is higher than for the side tamping method. In discrete element modeling, the performed laboratory tests were simulated. The compactness of the ballast bed, as well as the residual stresses, were determined in MATLAB. The side tamping technology provided five times higher residual stresses in the ballast layer below the sleeper than in the case of vertical tamping, which can be explained by the more stable and dense layer resulting from the side tamping ensures higher interlocking between the grains. The simulation of the wave propagation shows an influence of the residual stresses on the wave propagation velocities. The simulated wave propagation velocity was more than two times higher for the side tamping than for the vertical one.

1. Introduction

Today, mainly in the last decades, railroad transportation will have a significant role in development and civilization. In the 1800s and 1900s, more and more railway lines were constructed worldwide [1].

There were main tasks that had to be solved, e.g., developing the hauling force of the railway engines; continuously changeover to diesel and electric operation instead of steam hauling [2]; the increased need for speed on the railroads [3]; etc. Environmentally safe techniques and methods (decreased pollution, decreased demand for energy, use of renewable sources during operation, etc.), the economic solutions (optimized lifetime costings, etc.) came into the front [4].

Regarding the objectives as mentioned earlier, the following ones can be noted: use of damping courses and materials [5–7]; providig reduced stress in the track and beneath elements that proceed reduced deformation [8,9]; technologies that ensure specific work mechanisms, e.g., side tamping that doesn't disrupt the compactness of ballast course beneath the sleepers [10]; developed methods and techniques provide lower dynamic impacts that can cause supplementary track defects (cracks, breakage, etc.) [11–13]; reducing the wear of rails and other parts of the track [14–18]; inspection and monitoring of railway infrastructure [19–21], using of recycled and reclaimed materials [22], etc.

There is another 'trend' considering railroad infrastructure development: the enhancement of railroad networks regarding interoperability across borders between states [23].

Railway track condition and the maintenance costs depend first of all

* Corresponding author.
E-mail addresses: michal.przybylowicz@mailbox.tu-dresden.de (M. Przybyłowicz), mykola.sysyn@tu-dresden.de (M. Sysyn), ulf.gerber@tu-dresden.de (U. Gerber), kovalchuk.diit@gmail.com (V. Kovalchuk), fischersz@sze.hu (S. Fischer).

https://doi.org/10.1016/j.conbuildmat.2021.125708
Received 23 July 2021; Received in revised form 5 October 2021; Accepted 12 November 2021
Available online 24 November 2021

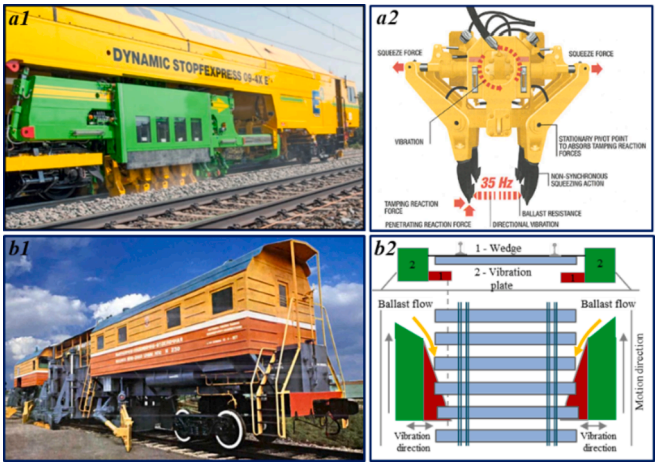

Fig. 1. The vertical and side tamping techniques (a1 – tamping machine Dynamic Stopfexpress (i.e., dynamic tamping express) 09-4X [24], a2 – vertical tamping unit of 09-4X [24], b1 – tamping machine VPO-3000 [30,31], b2 – horizontal tamping unit of VPO-3000).

on the development of track geometric irregularities. The most influencing cause of the irregularities is the inhomogeneous settlements of the ballast layer under the operation loading due to dynamic impacts, ballast compaction inhomogeneity, subgrade stiffness variation, etc. [24,25]. The accumulation of track geometrical irregularities over the demands of the admissible level cost expensive maintenance work and traffic hindrance. According to the studies [26,27], about 40% of its operating budget on track maintenance is related to ballasted track maintenance and renewal. The high ballast maintenance costs arise not only due to frequent corrective tamping with the average tamping cycle of about 40–70 million gross tonnes (Mt or MGT) [26] but also due to expensive ballast cleaning (in other words: ballast screening).

There are two principal ways of mechanized track geometry correction: ballast tamping and mechanized and non-mechanized stone blowing technologies. In turn, the current ballast tamping methods that have found a practical application are based on the vertical and side tamping techniques. Most tamping machines worldwide exploit the vertical tamping technique that is usually implemented in the Plasser&Theurer [28] and Matisa [29] tamping machines (Plasser&Theurer is an American, hence Matisa is a Swiss company; the first tamping machine was introduced in the 1960s). The vertical tamping technique uses tamping tines (in other words: i.e., tamping 'hammers') that are penetrated in the ballasted trackbed between the sleepers (see Fig. 1 (a1, a2)). The vibration and squeezing with and frequency approx. 35–40 Hz and pressure 11.5–12.5 MPa cause liquefaction of ballast material and void filling under the lifted sleepers (there were machines in the past which were able to lift and tamp only one sleeper at a time; after that, the common machines can solve this procedure with two sleepers simultaneously, since the 2010s there are machines with 3 and 4 sleepers techniques already. Nowadays, the Plasser 09-4X machines and their subtypes are the quickest and most productive tamping machines).

The side tamping technique applies wedge-shaped plates that are continuously moved on both sides along the railway track axis. The horizontal vibration causes the movement and compaction of crushed stone under the lifted sleepers. The side tamping method is still applied for the ballast tamping on the railways of CIS states (Commonwealth of Independent States) in the machine of type VPO (combined alignment, tamping, and ballast distribution) (see Fig. 1(b1, b2)) [30,31]. The stone blowing technology is based on air blowing of small stone particles underneath the voided sleeper. The method is applied by some railway companies in Great Britain, Spain, and the USA [24,32]. However, the technique uses heavily contaminated ballast tracks to prolong the life-cycle until the next ballast screening. Moreover, the application of the

Table 1
Comparison of the vertical and side tamping machines (based on [24,38,39]).

Tamping machine	Vertical tamping (Dynamic Stopfexpress 09-3X and 09-4X)	Side tamping VPO-3000
Maximal efficiency [m/h]	2000 (09-3X) 2400 (09-4X)	3000
Maximal lifting for in one phase [cm]	5	10
Accuracy of geometry after tamping [mm]	±1	±2
S&C tamping	yes	no
Wide sleeper(ed) track tamping	no	yes
Fine particles after tamping [kg/sleeper]	1.6–3.9	0.6
Contact area of tamping unit [m^2]	0.01	0.35
Tamping units pressure [MPa]	11.5–12.5	0.135

usual tamping machines on the tracks is not efficient due to the relatively high fine content below the sleepers. Therefore, the stone-blowing technology is not considered in the current comparative study.

The vertical and the side tamping techniques have different advantages and drawbacks. The vertical tamping method provides excellent geometrical quality, adequate ballast compaction, and high productivity. It can be used for ordinary track, as well as for switches and crossings (S&C). The key drawback is a high ballast material destruction (degradation) during the tamping (i.e., the tamping hammers break the particles during the process). Many studies confirm a significant influence of vertical tamping on the ballast particles breakage, defragmentation [33,34]. The ballast particles breakage with several tamping causes the acceleration of ballast permanent settlements and finally demands a cost-expensive ballast cleaning. The high particle destruction is caused by a high contact pressure of the tamping tines on ballast stones in the process of penetration in the trackbed and squeezing operation [35,36]. Additionally, the vertical tamping technique can be used only on the track with standard, ordinary sleepers.

The side tamping technique provides high productivity and low ballast particle breakage. This particle-saving tamping is caused by the low contact pressure of tamping units. The tamping can also be applied for slab tracks, and it should be mentioned that it is independent of sleeper type. The main disadvantage of the side tamping machine is that it is not an optimal tamping unit for geometrical corrective maintenance. Another shortcoming is the resulting geometrical accuracy of the track position. A possible improvement of the 'machine surfacing' of the rail track is presented in the study [37]. Therefore, the machine is usually utilized after ballast replacement or screening, where high track lifting and productivity are necessary. A comparison of the vertical and horizontal tamping technologies is shown in Table 1 [24,38,39].

The influence of the tamping technology on the ballast compaction is presented in the theoretical studies [40–42]. The studies demonstrate the results of DEM modeling of different tamping methods and different sleeper support conditions. The results show the significantly lower local porosity in the ballast layer under the sleeper after side tamping than after the vertical tamping technique. In addition, side tamping provides much more homogenous sleeper support conditions that significantly reduce ballast contact pressure, as shown in the study [43].

The DEM is widely used to study the ballasted track of the railway [17,44–50]. Some studies [40–42,51] used the DEM to simulate the tamping process. The residual stress in the ballast bed using DEM was studied in [52], as well as [53] investigated the effect of ballast particles' shape onto the ballast tamping and the lateral stability of the ballasted railway tracks using the discrete element method. [53] concluded that tamping significantly reduces (approx. with 40%) the lateral stability of the track, even if particles are quite angular and there are center-bound tie; flatness and elongation of a particle had only a minor effect on

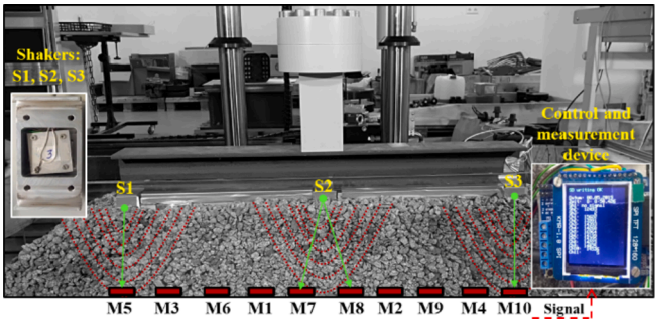

Fig. 2. The ballast layer model and the measurement system for compaction measurement: M1–M10 – MEMS accelerometers ADXL355; S1-S3 – electromagnetic shakers; Microcontroller ESP32 with TFT LCD module.

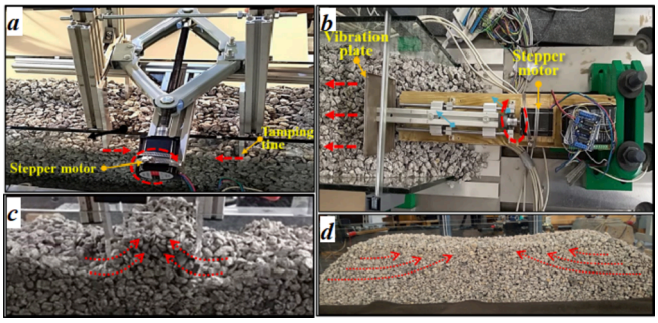

Fig. 3. The models of the vertical (a) and the horizontal (b) tamping units, as well as the ballast transportation with tamping units (c – vertical tamping, d – side tamping).

lateral stability since aggregate breakdown or degradation was not considered in their DEM analysis.

[54] studied the effect of the tamping operation on mechanical qualities of ballast bed using DEM-MBD coupling method. They investigated the compactness of the ballast bed in different depths under the sleeper during the tamping process, i.e., lift, insert, squeeze and retract, and the contact forces and ballast motions. After the vertical tamping process, the highest compactness was observed even under the sleeper (+7.56%), and the lowest was related to the ballast top section between the sleepers (−34.77%) – compared to the state(s) before tamping. The recommended ballast depth is 20 mm, according to the results of [54]. Similar results were driven by [55], who investigated the stress–strain condition below sleepers considering different train loadings.

The comparison is performed with different criteria: the effectiveness of the ballast filling under the sleeper and the sleeper sides, residual stress distribution in the ballast bed after tamping, and ToF (time of flight) wave propagation. Wave and strain propagations are also applied in railroad engineering [56], e.g., determination of the dynamic response of the railway tracks.

The objectives of this paper are:

i) to estimate the ballast layer compaction after the vertical and side ballast tamping techniques using wave time of flight (ToF) measurements;
ii) to explore the ballast settlement behavior after the tamping under the vibration loading of the sleeper;
iii) a numerical comparison of the vertical and side tamping methods of the ballast bed with a discrete element model, and the wave propagation during these tamping processes.

2. Methods and materials

2.1. Experimental set-up of the ballast layer and ballast tamping methods

The investigation is based on a scaled laboratory modeling of the ballast tamping supplemented by subsequent ballast settlement measurements under vibration loading acted on the sleeper. A ballast material is limited and 'supported' with fixed glass walls, and free front sides present the scaled model of the trackbed (see Fig. 2). The distance between the walls is 320 mm, and the thickness of the ballast under a sleeper is approx. 230–270 mm. The sleeper is presented with a steel H-profile with a length of 1000 mm and a width of 100 mm. The ballast material is a granite aggregate of 8/26 mm (d_{min}/d_{max}, i.e., the minimum and maximum grain size). The vibration loading on the sleeper is produced by a servo-hydraulic test machine ZWICK HB 160.

The glass walls allow the performance of the photogrammetric measurements of the particle flow during loading. The measurements of dynamic loading on the sleeper were vertical displacements, and ballast compaction distribution is executed and analyzed in the present paper.

The ballast compaction distribution along with the sleeper after the vertical and the side tamping process is assessed using elastic wave ToF (time of flight) measurements. The measurements are carried out automatically with a developed microcontroller device that includes on the sleeper foot mounted three shakers and the multiple sensors under ballast aggregate along with the sleeper. The sensors were ten pieces of M1-M10 MEMS type analog accelerometers ADXL355 appended with electronic analysis modules. A detailed description of the measurement method is presented in the paper [57]. Different from the measurements summarized in the paper, the current measurements allow to perform the measurements without sleeper removal and during the loading of the sleeper.

2.2. The models of ballast tamping units

The scaled models of the vertical and side tamping units are developed. The models provide the transportation of the ballast material in the zone under the sleepers, similar to during machine tamping with vibration loading.

The model of the vertical tamping unit consists of two frames with tamping hammers (see Fig. 3 (a, c)). The frames are moved one to another with the help of a scissors mechanism that is driven with a stepper motor rotating a screw thread. The stepper motor is powered and controlled by a programmable microcontroller and a stepper driver. The controller is programmed to move the tines with a translation motion of 4 cm and vibration one with 35 Hz. Thus, the cyclic motion is similar to sinusoidal. The tines are manually penetrated in the ballast layer and with a removed sleeper.

The model of the side tamping unit is shown in Fig. 3 (b, d). This model, like the model for the vertical tamping, is driven with the stepper motor. However, the horizontal translational motion is higher than the vertical tamping model and corresponds to the real tamping unit. The height of the ballast moved with the vibration plate was considered in 2 variants: 13 cm and 6 cm deep tamping. The second variant would correspond to the possible improvement of the present side tamping unit for the geometrical corrective tamping. The authors demonstrated the results for the first variant of side tamping in this paper.

2.3. Calibration of the method for ballast compaction measurements

The calibration was carried out to determine the relationship between the measured pressure wave ToF and ballast density. The calibration was performed in the same experimental set-up but with a limited ballast box 320 × 270 × 270 mm (see Fig. 4) with three cases of compaction. Within each case, the wave velocity was measured and recorded.

In the first case, the ballast layer had the lowest compaction (density) that was solved by a simple filling into the ballast box. The ballast compaction in the second case was produced with manual impacts on

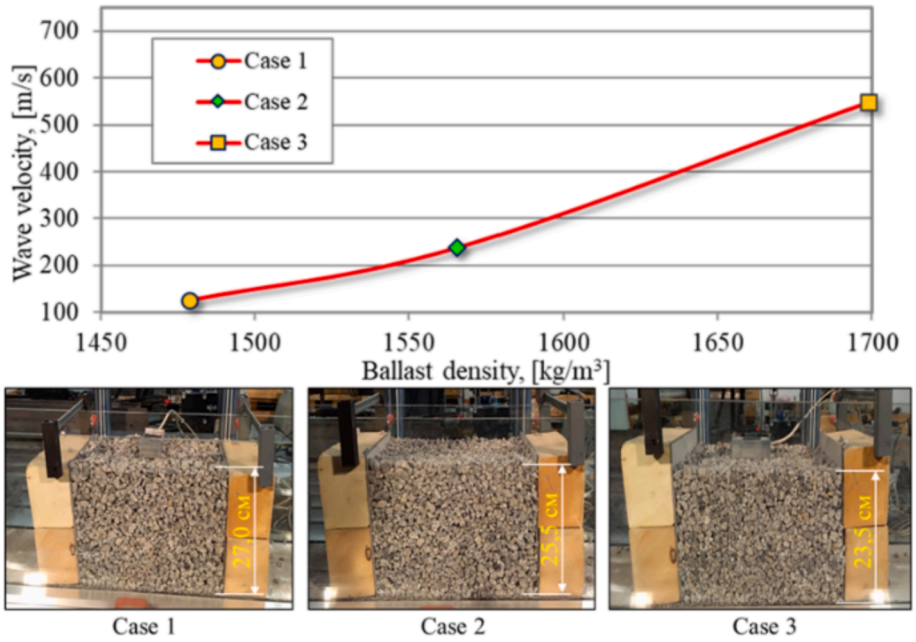

Fig. 4. Calibration of the method for ballast compaction measurements: Case 1 – uncompacted ballast; Case 2 – intermediate compaction in one layer; Case 3 – maximal layer by layer compaction.

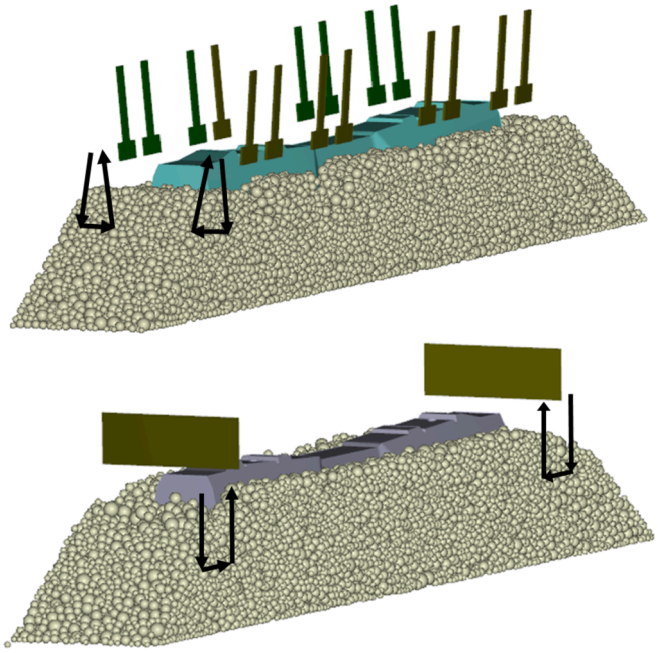

Fig. 5. Ballast bed after the vertical (top) and side tamping (bottom) cycle.

the upper free surface. Thereby, the settlement from 27 cm to 25.5 cm was obtained. The maximal compaction of the ballast layer was reached in the third case after compaction with multiple layers of height about 7 cm. The reached maximal ballast settlement was approx. 3.5 cm. The wave velocity and ballast density were calculated based on the calibration measurements. Fig. 4 shows the relationship between wave velocity and ballast density. The mean wave velocity for compacted ballast is 124.4 m/s, for the intermediate compaction, it is 237.14 m/s, and for the maximal, it reached 548.2 m/s. The corresponding ballast density is 1478.75 kg/m^3 for the uncompacted ballast, 1565.74 kg/m^3 for the intermediate compaction, and 1698.99 kg/m^3 for the maximal compaction reached.

The received results of the ballast velocity calibration are similar to the same results of the other studies [57,58], where the pressure wave velocity in the crushed rock was measured between 100 m/s and 650 m/s depending on its compaction degree.

2.4. Numerical modeling of tamping processes and wave propagation

The aim of the section is a numerical comparison of the vertical and side tamping methods of the ballast bed. A discrete element model is used for the simulation.

Thus, the estimation in this study is produced using a DEM algorithm to simulate residual settlements of one sleeper in a ballast box under the tamping loadings of vertical (Fig. 5, top) and side (Fig. 5, bottom) cases in MATLAB [59]. The vertical tamping is produced by eight pairs of tamping tines that move both rotational and translational. The side tamping is depicted with two plates that translationally move the ballast under the sleeper ends. The movement is both rotational and translational. Both the tines and plated move together with vibration 35 Hz. The tamping begins after the sleeper is uplifted to 50 mm. The sleeper geometry corresponds to the B70 type sleeper.

The particles form is simple ball(s) with the size standard distribution of 22.4–63 mm. The model's mechanical parameters were derived with the model calibration to the accurate model with the natural form particles [60,61]. Thus, the applied model is dimension reduced one having the advantage of quick simulation that is important for the simulation the settlement accumulation requiring many loading cycles to receive the definite settlement intensities. The number of the particles is 29,788. The particle material properties correspond to the granite rock are the following: static friction 0.56, dynamic friction 0.54, restitution coefficient 0.72, bulk density 1700 kg/m^3, Young Modulus 50 GPa, Poisson ratio 0.3, rolling resistance 0.38. The sleeper and the subgrade properties are the following: static friction 0.56, dynamic friction 0.54, restitution coefficient 0.72, density 2650 kg/m^3, Young-modulus 20 GPa, Poisson ratio 0.3. The rolling resistance model corresponds to the elastic–plastic approach [62] that considers rolling radii, the tangential stiffness, rolling resistance coefficient, etc. The tangential force model is a Mindlin-Dersiewicz model. The normal force model is a Hertzian spring with viscous damping.

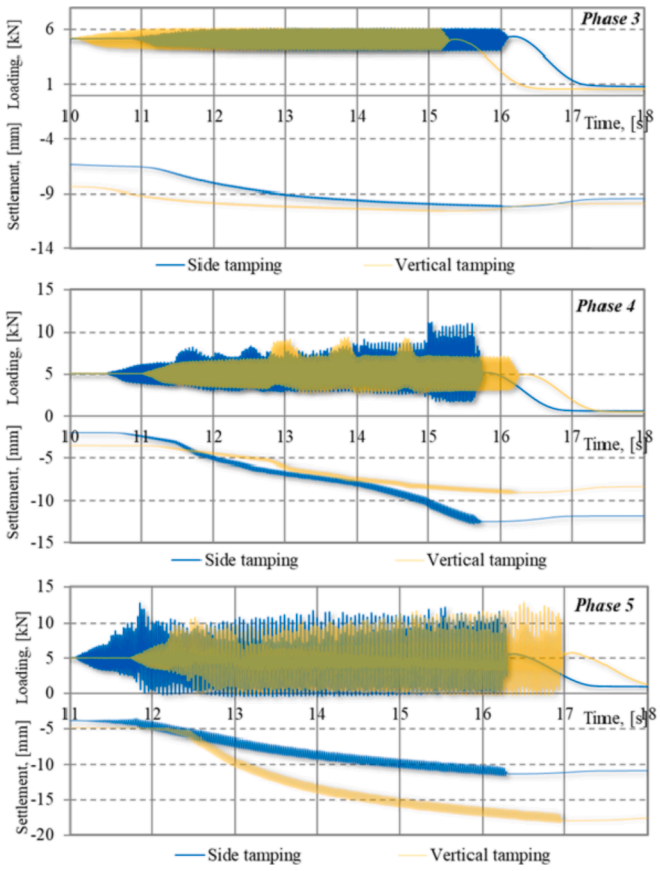

Fig. 6. Ballast settlements during the phases 3–5 of the experiment.

3. Results and discussion

3.1. Experimental measurements of ballast layer settlements after tamping

The program of the experimental investigation consists of five phases of the ballast loading and the subsequent measurement of the wave velocities in the ballast under the sleeper. The five (loading) phases were as follows:

1. Ballast bed filling with uncompacted ballast material (the same for the vertical and horizontal tamping).
2. Tamping operation in the compacted trackbed.
3. Vertical permanent loading on the sleeper 5 kN and 200 cycles of 40 Hz sinusoidal cyclic loading with amplitude 1 kN.
4. Vertical permanent loading on the sleeper 5 kN and 200 cycles of 40 Hz sinusoidal cyclic loading with amplitude 2 kN.
5. Vertical permanent loading on the sleeper 5 kN and 200 cycles of 40 Hz sinusoidal cyclic loading with amplitude 5 kN.

Phases 3–5 correspond to the stabilization of the ballast layer after tamping. Fig. 6 shows the ballast bed's comparative loading and settlement behavior for the vertical and side tamping.

The ballast settlements in the third phase of the experiment were 3.8 mm for the side tamping and 1.8 mm for the vertical one. The settlements during the vibration loading are also considered. Both settlement lines demonstrate the decay of the settlement intensity.

The fourth phase was characterized by unstable dynamic loading of the sleeper and, therefore, its influence on the settlement behavior. In general, the settlement intensity after both tamping cycles is about the same. The increase of the settlements after the 14 s of the vibration is related to the growth of the loading. The sleeper settlement after the vertical tamping was 7 mm; hence after the side one was 13 mm.

In the last experiment phase, the dynamic loading was as high as the static part; the sleeper was completely unloaded. It causes intensive

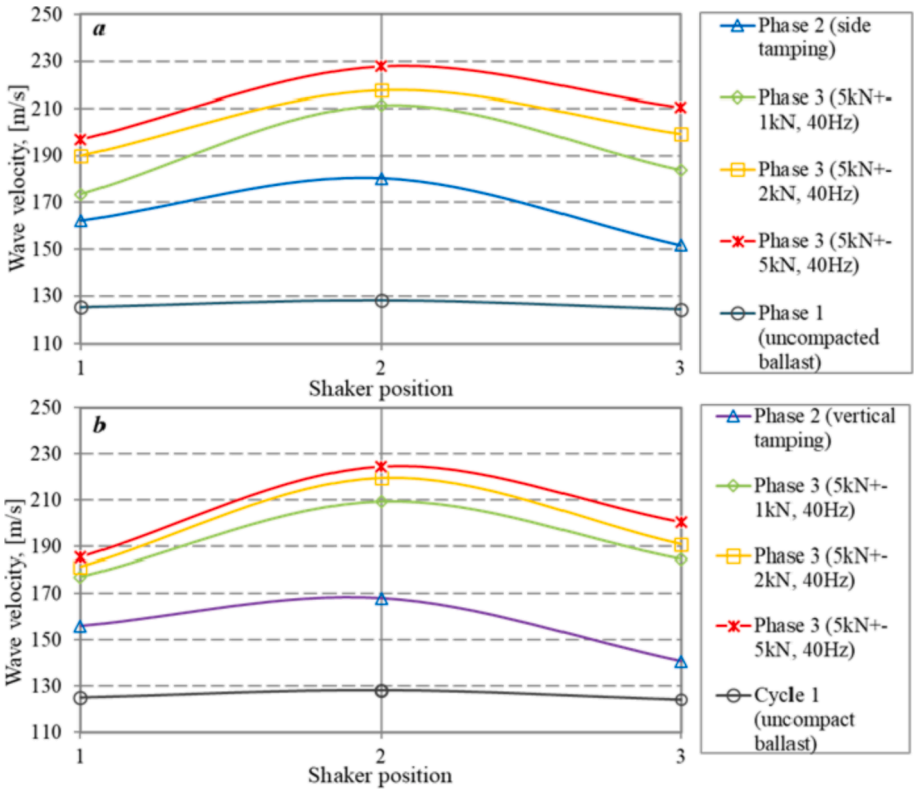

Fig. 7. The velocities of wave propagation in the ballast layer after side tamping (a) and vertical tamping (b), as well as the stabilization phases.

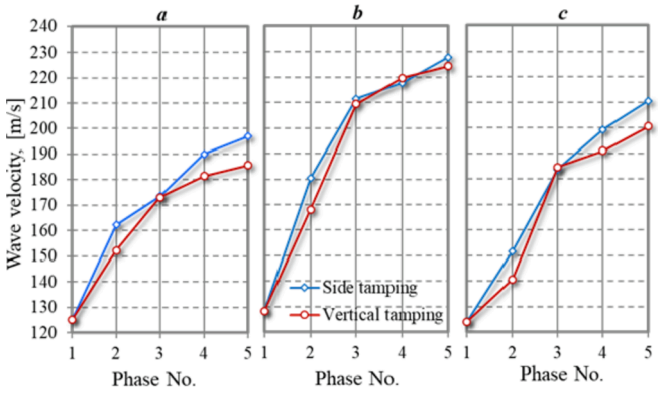

Fig. 8. Comparison of the wave velocities in the ballast layer depending on the ballast zone and tamping method: a – left end of the sleeper; b – sleeper center; c – right end of the sleeper.

settlements of the ballast layer. Different from the previous 2 phases, the ballast settlements for the vertical tamping were higher than for the side tamping method. The intensity of the settlement during the last vibration phase for the vertical tamping method was 2.6 mm/100 cycles; hence for the side tamping, it was 1.7 mm/100 cycles. The different ballast bed behavior in the last experiment phase could be explained with the influence of different factors: the local support of the sleeper at both ends during the vertical tamping, the different ballast compaction (and some loosening) related to the other tamping method.

3.2. Experimental measurements of compactness of ballast layer after tamping

Ballast layer compactness is determined after each of the five tamping cycles of the experiment. The ballast compaction after the first cycle for the most uncompacted ballast is considered the same for both tamping variants. Therefore, only vertical wave rays between the shakers and sensors are deemed to be shown in Fig. 2. The reduction of the ballast height after each loading cycle is taken into account for the wave velocity calculation. Fig. 7 depicts the wave velocities in the ballast layer under the ends of the sleeper and its middle point for the tamping methods and the subsequent stabilization.

Both diagrams in Fig. 7 demonstrate a significant increase of wave velocities in the ballast layer after the tamping and stabilization phases compared to the uncompacted ballast layer. It should be noted that the tamping phases were performed at an already stabilized ballast layer. Thus, the tamping produces some reduction of the compactness. The mean wave velocity in the central part of the trackbed was 168.1 m/s for the vertical tamping and 180.4 m/s for the side one (1.00:1.073). The velocities increased to 209.4 m/s and 211.5 m/s, correspondings to both tamping methods after the ballast stabilization in phase 3 (1.000:1.010). The following phase 4 of the experiment provided a non-significant increase in the ballast layer compactness under the sleeper's middle part. The maximal wave velocity in the intermediate zone of the ballast layer after the vertical tamping was 227.9 m/s and 224.38 m/s for the side tamping (1.000:0.985). Thus, the compactness in the middle zone of the trackbed was almost the same for both tamping techniques. The comparison of the wave velocities under the sleeper center and its ends for both tamping methods is demonstrated in Fig. 8.

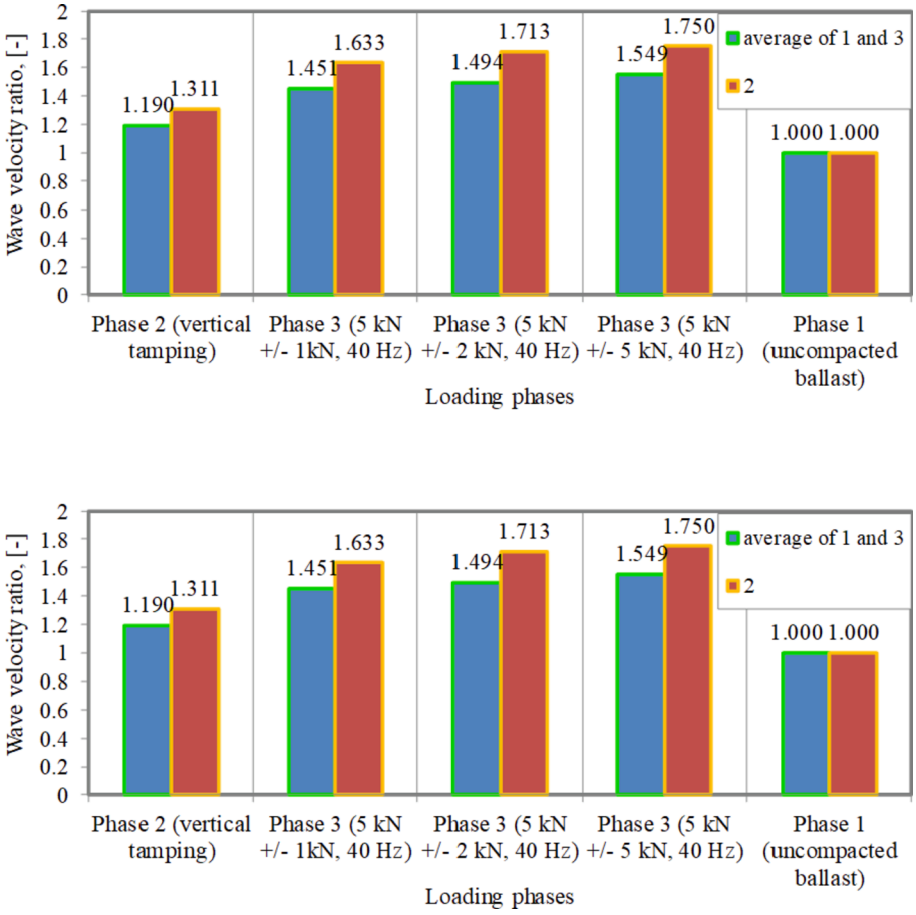

Fig. 9. Wave velocity ratios with the consideration of average value below sleeper ends, as well as sleeper center (top – side tamping; bottom – vertical tamping; the reference values are related to Phase 1 (uncompacted ballast)).

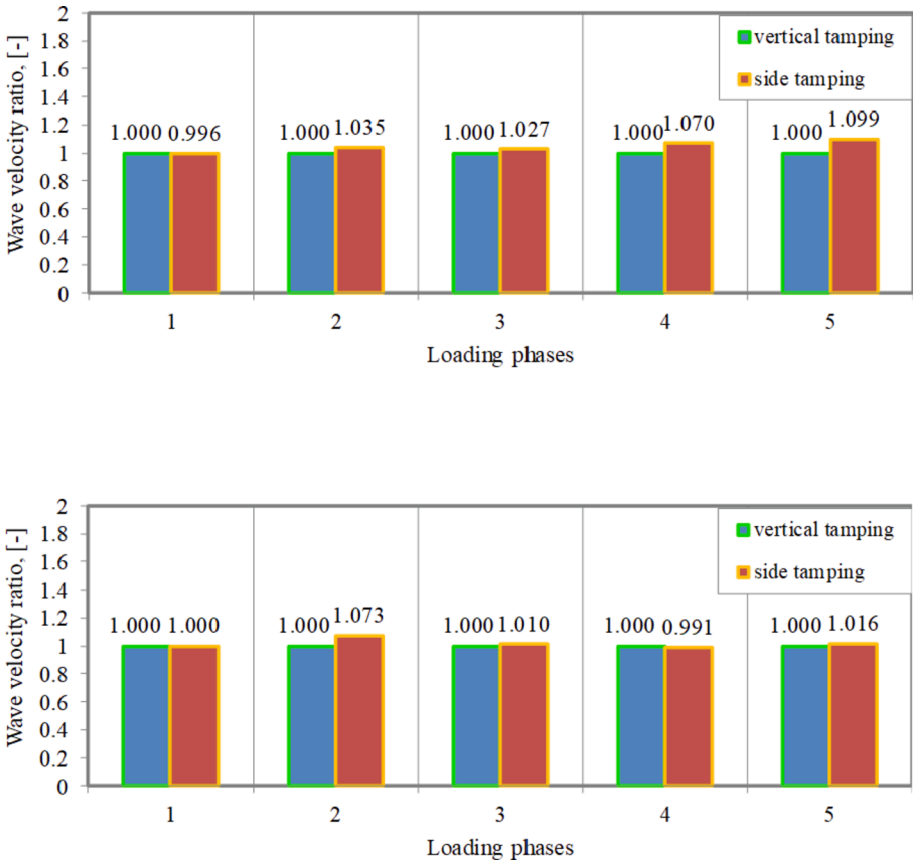

Fig. 10. Wave velocity ratios with the consideration of loading phases, as well as tamping methods (top – average value of below sleeper ends; bottom – sleeper center; the reference base is the value related to vertical tamping at Phase 1).

Different compactness values were inspected under the central part of the sleeper and under the sleeper's ends with the wave velocities measurements. After the vertical tamping, the wave velocities were 156.0 m/s for the left side and 140.7 m/s for the right side of the sleeper (1.109:1.000). Whereas after the side tamping, the velocities are higher and amount correspondingly to 162.2 m/s and 151.7 m/s (1.069:1.000). Thus the ballast compactness after the side tamping was about 7% higher than for the vertical tamping. However, the mean wave velocities after the ballast stabilization in phase 3 were almost equal for both tamping methods. The high increase of ballast compactness for the vertical tamping can be explained by the leveling of the ballast material that was unevenly transported with the tamping tines. The further stabilization in phases 4 and 5 caused the increase of the compactness under both sleepers' ends. However, the increase of the wave velocity was different for the ballast layers tamped with different methods. After phase 5, due to the high dynamic loading, the wave velocity amounted to 185.7 m/s and 200.5 m/s at both sleepers' ends for the vertical tamping method (1.000:1.080). The velocities in the same zones for the side tamping method were 196.93 m/s and 210.6 m/s (1.000:1.070). Thus, the side tamping caused about 5–7% higher wave velocity and better compaction than the vertical tamping method. However, the difference was relatively low significant due to the high variation of measurement data. The difference can be explained with more homogenous ballast compactness and ballast height after the deep side tamping. On the other hand, the vertical tamping produced a local accumulation of ballast material at the end of sleepers and, at the same time, local ballast loosening. This fact is indirectly confirmed with a higher settlement intensity (Fig. 6) after the last phase for the vertical tamping case. The long-term cyclic tests and the photogrammetric measurements of ballast flow could receive a more insightful answer related to the better tamping method. These experimental studies are promising for future researches.

In Fig. 9, the authors summarized their relevant results related to the introduced laboratory tests. In Fig. 9, the values that represent the results on sleeper ends are average values of the left and right sides. Fig. 9 gives the calculated ratios where the reference base is the uncompacted state (i.e., phase 1). It is another depiction of Fig. 7.

In Figs. 10 and 11, the results of Fig. 8 are represented similar to Fig. 9; hence there the reference base is the vertical tamping: in Fig. 10, the reference base is the values related to vertical tamping at each phase; in Fig. 11, the reference base is the value related to vertical tamping at Phase 1. Figs. 10 and 11 show the wave velocity ratios categorically to each case.

3.3. Discrete element modeling

3.3.1. Ballast tamping

Fig. 12 presents the particles' trajectories during the tamping cycles for two tamping cases. Both diagrams show that the particles are filling the void zone that appears after the sleeper lifting. However, the sizes of the particle flow zones are different. The flow zone for the vertical tamping is located in the upper part of the ballast layer. The bottom 10 cm of the ballast is not disturbed. Thereby, the flow zone for the side tamping case is distributed over the whole ballast layer. Moreover, the particle flow is present under the middle part of the sleeper.

Analysis of the sleeper support after the tamping shows adequate particles filling the void zone (Fig. 13). However, the sleeper support for the vertical tamping case presents a small partially supported zone under the middle part of the sleeper outside of the tamping tines zones. Additionally, the ballast filling between the sleepers and at both sides of the sleeper (Fig. 5) is different.

Comparing the residual normal loadings on the particles after the

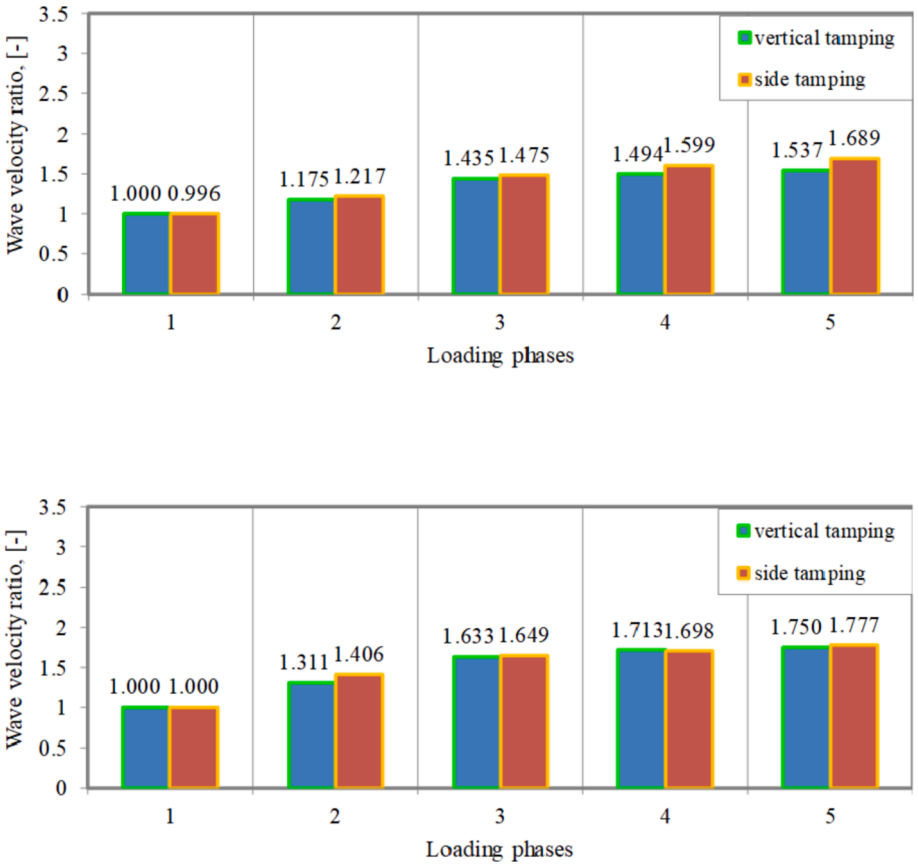

Fig. 11. Wave velocity ratios with the consideration of loading phases, as well as tamping methods (above – average value of below sleeper ends; below – sleeper center; the reference base is the value related to vertical tamping at Phase 1).

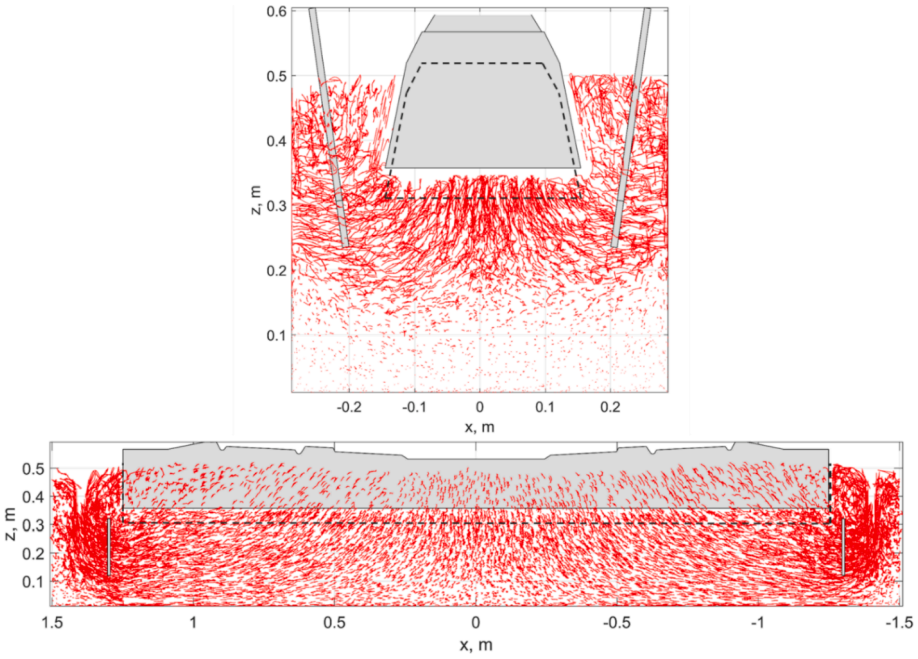

Fig. 12. Ballast particle trajectories during the vertical (top) and side tamping (bottom) cycle.

tamping cycles (Fig. 14) shows quite different results. Fig. 14 presents the particles that carry more than 5% normal loading of the maximal one for the side tamping case. The particles colors from blue to red corresponds to the loading variation from 5% to the maximal loading. It is clear that the stressed zone after the side tamping is much bigger than for the vertical tamping. This is because the maximally stressed zones are located at the bottom of the ballast bed.

The quantitative comparison of the normal loading distribution

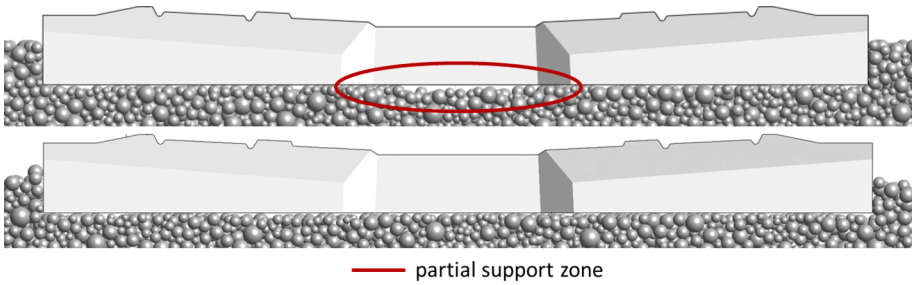

Fig. 13. Ballast particle filling the void after the vertical (top) and side tamping (bottom) cycle.

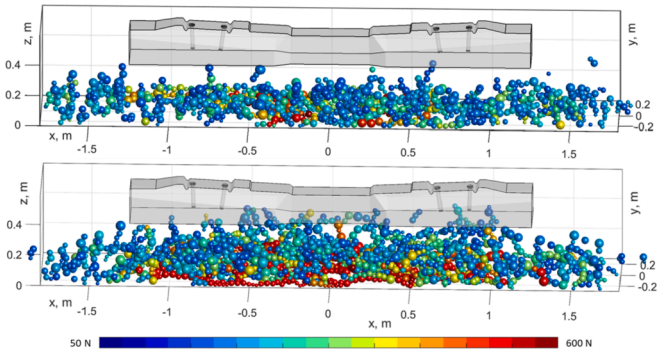

Fig. 14. Ballast particle subjected to significant (>5% of maximal) normal loadings after the vertical (top) and side tamping (bottom) cycle.

along the sleeper is presented in Fig. 15. The grey points correspond to the particles loading at the x-coordinate along with the sleeper. The maximal particle loadings are concentrated under the middle part of the sleeper. The loadings after the side tamping are more than three times higher than for the vertical tamping.

The analysis of the mean normal loading along the sleeper (red line) allows identifying different zones of the loading. The down part of the loading corresponds to the own weight of the particles and the sleeper. Over the gravitational zone are the zones with the parabolic increase of the normal loading (blue line). The middle part of the line can be described with a horizontal line. The loading part is the residual loading. A similar process of the residual stresses was experimentally determined and analyzed in the paper [63]. The comparison of the residual normal loadings of the particles shows that the parameter for the side tamping is about 5 times higher than for the vertical tamping. The reason can be the higher compactness that can be reached in the ballast layer by the side tamping: the produced more stable 'particle-skeleton' structure (of the ballast layer) ensures the higher interlocking between the grains, as well as the higher residual stresses (see Figs. 14 and 15).

3.3.2. DEM simulation of the elastic wave propagation under impact loading

The previous section shows the evident differences in the stressed state of the ballast bed after the different tamping methods. However, the residual stresses are difficult to control in practical applications. Nowadays, different non-destructive methods are proposed in the studies [57,64–66] to control the material state using a kinematic interpretation of wave propagation. Other studies [67,68] propose the dynamic interpretation of propagated waves in the ballast layer to evaluate its compaction. Modeling the wave propagation in the track and the ballast bed is usually presented by FEM or BEM (i.e., finite element method and boundary element method) methods in the studies [69–71]. Another promising approach time-effective simulation, is based on the wave theory of stress propagation or wave ray theory that is presented by studies [56,72]. However, the simulations are concerned with the continuous media, but the ballast layer is a discrete one with a high variation of the grail geometrical properties. Therefore, in the present study, the properties of the elastic wave propagation in the compacted ballast layer are studied in this section. The same DEM model is used for modeling the impact test. The loading is brought in the under-rail zone of the sleeper over the area 10 × 10 cm in a short time (Fig. 16). The wave propagation over the particles is studied.

The wavefront propagation in the different time moments after the impact for two tamping methods is shown in Fig. 17. The particles with an impact velocity of more than 0.1% of the maximal one are visualized. Additionally, the different absolute velocity is shown within a blue-red colormap. Both diagrams show the increase of the velocity front sizes during the time. However, the front sizes and form for the vertical and the side tamping ways are different. In the overall comparison of the front sizes for the vertical (Fig. 17, left) and the side tamping (Fig. 17, right), the volume of the wavefront for the side one is noticeably more extensive than for the vertical tamping. The wave propagation front for the vertical tamping has a spherical form typical for the homogenous media. Thereby, the wavefront for the side tamping is stretched horizontally along with the sleeper with the prevailing direction to the ballast bed middle side.

Additionally, combinations of particles can be observed that correspond to the stress transmission three that is typical for the compacted ballast material. It is evident that the wave propagation speed for vertical tamping is higher. A possible explanation of the inhomogeneous wave propagation with acceleration in the direction inside the ballast bed middle part could be the different ballast material compaction due to the other stressed states (Figs. 14 and 15).

The quantitative estimation of the vertical components of the wave velocities along the ballast bed depth under the impact location is presented as the conventional geotechnical diagrams in Fig. 18. The ballast wave arrival moments lines over the ballast depth correspond to the velocities. Despite some outliers in the wave ToF, there are clear trends of the first wave within the depth 20–35 cm. Therefore, the waves could be interpreted as pressure waves. The wave velocity for the side tamping is about 36% higher than for the vertical tamping. The velocities correspond to the reference literature [58] for the rock materials. The outliers could be explained on the one side with the different lateral particle positions in the considered vertical ballast column under the impact position. On the other side, Fig. 17 shows clearly that the wave path is not straight. Therefore, the conventional geotechnical presentation should be considered as very approximate. The wave propagation under the 20 mm depth shows a wave dispersion. The quite distinct dispersion for Fig. 18, right, could be interpreted as the shear wave. The evident absence of the shear wave in Fig. 18, left could be supposed with its long delay that is outside the diagram time range. The experimentally measured ToF could be explained as the shear waves arrivals. However, it should be noted that the experimentally measured low ToFs using the low-frequency accelerometers ADXL355 could be subjected to the systematic error due to the measurement time delay compared. Thus, the absolute wave velocities in the experiment and in the simulation are not directly comparable.

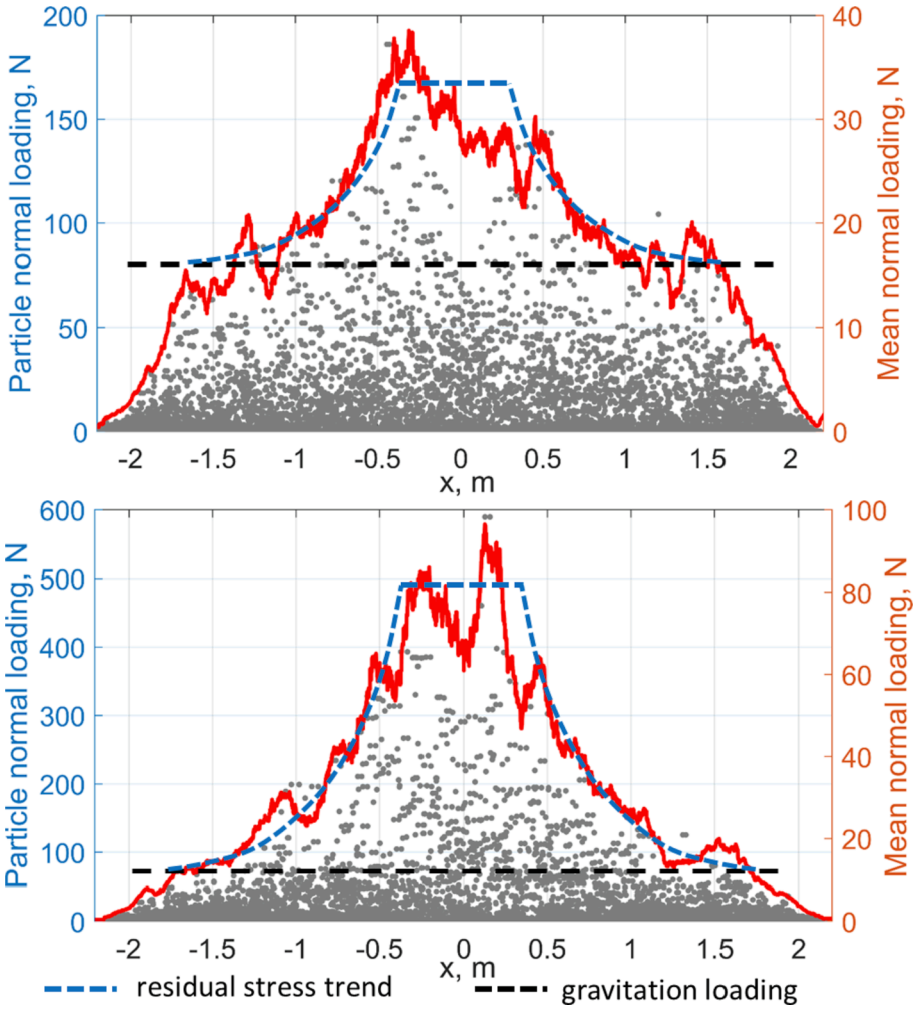

Fig. 15. Ballast residual pressure distribution along with the sleeper after the vertical (top) and side tamping (bottom) cycle.

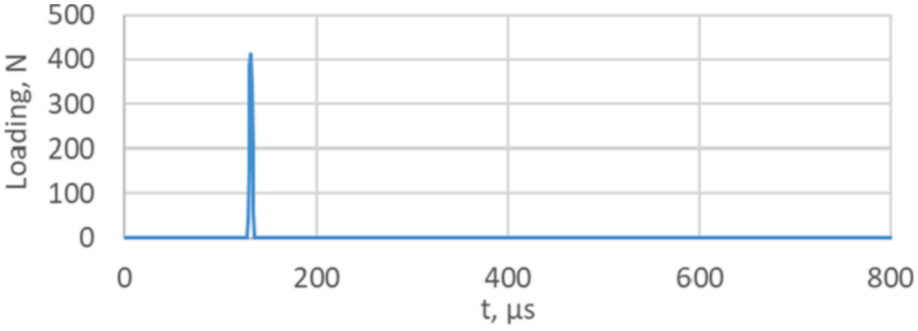

Fig. 16. Wave propagation velocity field for the case of vertical tamping.

4. Conclusions and further research possibilities

This study evaluated ballast layer compactness and the ballast layer settlements considering two tamping methods; were vertical tamping and side tamping technologies. The following conclusions can be drawn based on the prepared investigation (laboratory tests):

1. Maximal compactness of the ballast layer can be achieved under the middle part of the sleeper, and it does not depend on the method of ballast compaction.
2. The ballast compactness under the sleeper ends is up to 18% lower than under the central part of the sleeper; it is certified that it highly depends on the ballast tamping method.
3. The pressure wave velocity in the ballast under both sides of the sleeper is 5–7% higher for the side tamping method than for the vertical tamping.
4. Ballast settlement intensity after the vertical tamping is higher than after the side tamping; the approximate ratio is about 2.0.

The authors received valuable results and experiences with the discrete element modeling; the main results are the following:

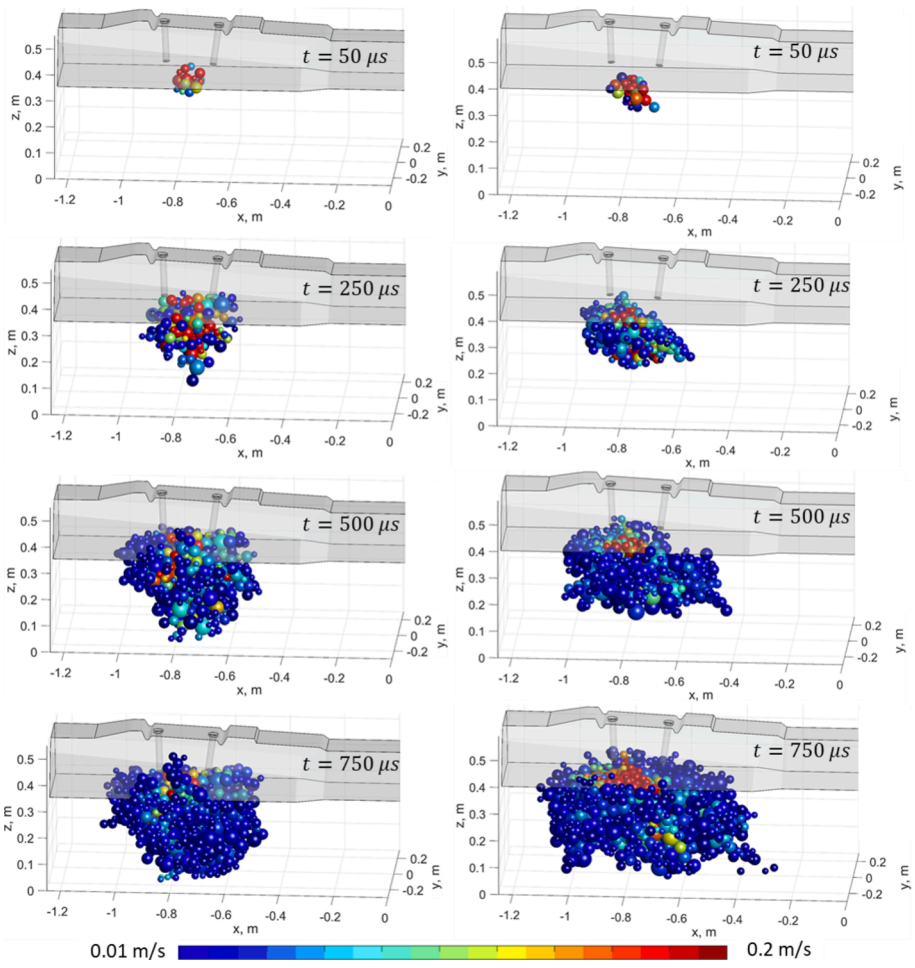

Fig. 17. Wave propagation velocity front for the case of vertical tamping (left column) and side tamping (right column).

1. The DEM was adequate for simulation of the executed laboratory tests in MATLAB; both the deformation (displacement) of the system, both the compactness of the ballast layer were able to be modeled.
2. After the side tamping, there was no void zone below the sleeper's center, which results in modified support conditions that have to be considered in the design phase of the reinforced concrete sleepers due to the flexural crackings at the top center of the sleepers because of the high negative bending moment.
3. The comparison of the residual normal loadings of the particles showed that the parameter for the side tamping is about five times higher than for the vertical tamping. The reason can be the higher compactness that can be reached in the ballast layer by the side tamping: the produced more stable 'particle-skeleton' structure ensures the higher interlocking between the grains and the higher residual stresses.
4. The wavefront propagation in the different time moments after the impact for two tamping methods was calculated. The quantitative estimation of the vertical components of the wave velocities along the ballast bed depth under the impact location was presented as the conventional geotechnical diagrams, which are only approximations. The ballast wave arrival moments lines over the ballast depth correspond to the velocities.
5. Despite some outliers in the wave ToF, there are clear trends of the first wave within the depth 20–35 cm. The waves could be interpreted as pressure waves. The wave velocity for the side tamping is about 36% higher than for the vertical tamping.
6. The outliers could be explained on the one side with the different lateral particle positions in the considered vertical ballast column under the impact position. The wave propagation under the 20 mm depth shows a wave dispersion. The quite distinct dispersion of the ToF results, right could be interpreted as the shear wave. The evident absence of the shear wave could be supposed with its long delay that is outside the diagram time range.

The authors set themselves the aim to continue their research as improvements:

1. The tamping methods can be investigated and assessed by photogrammetric measurements of ballast flow during long-term cyclic tests.
2. Advanced discrete element models can be built in which different PSD (particle size distribution) of ballast aggregate, sophisticated particle shapes, accurate vehicle loading characteristics, etc., can be considered.
3. Field tests to be able to validate laboratory tests, as well as discrete element models.

CRediT authorship contribution statement

Michał Przybyłowicz: Investigation, Visualization. **Mykola Sysyn:** Conceptualization, Methodology, Validation, Resources, Project administration, Writing – original draft. **Ulf Gerber:** Supervision. **Vitalii Kovalchuk:** Software, Formal analysis, Data curation. **Szabolcs Fischer:** Writing – review & editing.

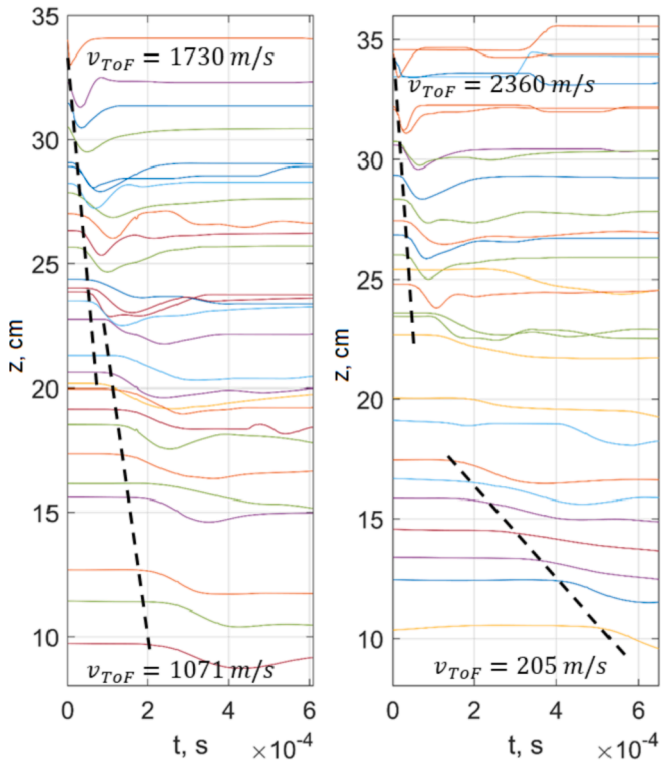

Fig. 18. Particle velocities in the ballast bed under the impact position for the vertical (left) and side tamping (right).

Declaration of Competing Interest

The authors declare that they have no known competing financial interests or personal relationships that could have appeared to influence the work reported in this paper.

Acknowledgements

The authors would like to acknowledge the following staff members of Chair of Planning and Design of Railway Infrastructure who have made this study possible, namely Head of laboratory the Railway Construction Laboratory Dipl.-Ing. (FH) Stefan Dehne, for the support with the experimental investigations.

References

[1] A. Lakatos, P. Mándoki, Sustainability analysis of competition in public transport systems: a comparative case study in hungary and finland, Period. Polytech. Civ. Eng. 64 (2020), https://doi.org/10.3311/PPci.14824.
[2] Vladimir V. Sinyavski, Mikhail G. Shatrov, Vladislav V. Kremnev, Pronchenko Grigori, Forecasting of a boosted locomotive gas diesel engine parameters with one- and two-stage charging systems, Reports Mech. Eng. 1 (2020) 192–198, https://doi.org/10.31181/rme200101192s.
[3] M. Kazemian, F. Astaraki, M.M. Rad, A. Taheri, Condition monitoring of vibration at weak parts of rail for ballasted railway tracks in Iran, J. Korean Soc. Railw. 24 (2021), https://doi.org/10.7782/JKSR.2021.24.6.544.
[4] M. Jahangiri, J.A. Zakeri, Dynamic analysis of two-lane skewed bridge and high-speed train system, Period. Polytech. Civ. Eng. 63 (2019), https://doi.org/10.3311/PPci.13135.
[5] G. Csortos, F. Augusztinovicz, L. Kazinczy, Examination of rail dampers with respect to noise and vibration mitigation, Period. Polytech. Civ. Eng. 64 (2020), https://doi.org/10.3311/PPci.13382.
[6] K. Alireza Jahan Tigh, D. Marinkovic, M. Zehn, Parametric investigation of a rail damper design based on a lab-scaled model, J. Vib. Eng. Technol. 9 (2021) 51–60, https://doi.org/10.1007/s42417-020-00209-2.
[7] L. Ižvolt, P. Dobeš, M. Mečár, Testing the suitability of the extruded polystyrene (Styrodur) application in the track substructure, Acta Polytech. 60 (2020), https://doi.org/10.14311/AP.2020.60.0243.
[8] M. Sysyn, V. Kovalchuk, U. Gerber, O. Nabochenko, A. Pentsak, Experimental study of railway ballast consolidation inhomogeneity under vibration loading, Pollack Period. 15 (2020), https://doi.org/10.1556/606.2020.15.1.3.
[9] P.J. Gräbe, B.F. Mtshotana, M.M. Sebati, E.Q. Thünemann, The effects of under-sleeper pads on sleeper-ballast interaction, J. South African Inst. Civ. Eng. 58 (2016), https://doi.org/10.17159/2309-8775/2016/v58n2a4.
[10] M. Przybylowicz, M. Sysyn, V. Kovalchuk, O. Nabochenko, B. Parneta, Experimental and theoretical evaluation of side tamping method for ballasted railway track maintenance, Transp. Probl. 15 (2020), https://doi.org/10.21307/TP-2020-036.
[11] V. Kovalchuk, M. Sysyn, U. Gerber, O. Nabochenko, J. Zarour, S. Dehne, Experimental investigation of the influence of train velocity and travel direction on the dynamic behavior of stiff common crossings, Facta Univ. Ser. Mech. Eng. 17 (2019), https://doi.org/10.22190/FUME190514042K.
[12] M. Sysyn, O. Nabochenko, V. Kovalchuk, Experimental investigation of the dynamic behavior of railway track with sleeper voids, Railw. Eng. Sci. 28 (2020), https://doi.org/10.1007/s40534-020-00217-8.
[13] M. Amine Benmebarek, M.M. Rad, Dem modeling of crushable grain material under different loading conditions, Period. Polytech. Civ. Eng. 65 (2021), https://doi.org/10.3311/PPci.17948.
[14] M. Kurhan, D. Kurhan, R. Novik, S. Baydak, N. Hmelevska, Improvement of the railway track efficiency by minimizing the rail wear in curves, IOP Conf. Ser. Mater. Sci. Eng. (2020), https://doi.org/10.1088/1757-899X/985/1/012001.
[15] S. Fischer, Breakage test of railway ballast materials with new laboratory method, Period. Polytech. Civ. Eng. (2017), https://doi.org/10.3311/PPci.8549.
[16] E. Juhasz, S. Fischer, Investigation of railroad ballast particle breakage, Pollack Period. (2019), https://doi.org/10.1556/606.2019.14.2.1.
[17] E. Juhász, S. Fischer, Tutorial on the fragmentation of the railway ballast particles and calibration methods in discrete element modelling, Acta Tech. Jaurinensis (2021), https://doi.org/10.14513/actatechjaur.00569.
[18] A. Németh, S. Fischer, Investigation of the glued insulated rail joints applied to CWR tracks, Facta Univ. Ser Mech. Eng. (2021) 7642, https://doi.org/10.22190/FUME210331040N.
[19] M. Banić, A. Miltenović, M. Pavlović, I. Ćirić, Intelligent machine vision based railway infrastructure inspection and monitoring using UAV, Facta Univ. Ser. Mech. Eng. 17 (2019), https://doi.org/10.22190/FUME190507041B.
[20] A. Kampczyk, K. Dybeł, Integrating surveying railway special grid pins with terrestrial laser scanning targets for monitoring rail transport infrastructure, Meas. J. Int. Meas. Confed. 170 (2021), https://doi.org/10.1016/j.measurement.2020.108729.
[21] A. Matejov, J. Šestáková, The Experiences with utilization of BIM in railway infrastructure in Slovak Republic and Czech Republic, Transp. Res. Procedia (2021), https://doi.org/10.1016/j.trpro.2021.07.084.
[22] M.H. Wayne, D.J. White, J. Kwon, J. Kawalec, Evaluation of reclaimed hydrated fly ash as an aggregate for sustainable roadway base material, Adv. Civ. Eng. 2021 (2021), https://doi.org/10.1155/2021/8756569.
[23] M. Kurhan, D. Kurhan, M. Husak, N. Hmelevska, The advisability of using dual gauge for expansion of the international traffic, in: Transp. Means - Proc. Int. Conf., 2020.
[24] B. Lichtberger, Track Compendium, Eurailpress Tetzlaff-Hestra GmbH Co. Publ., Hamburg, 2005.
[25] S. Fischer, Investigation of effect of water content on railway granular supplementary layers, Nauk. Visnyk Natsionalnoho Hirnychoho Universytetu. 2021 (2021). https://doi.org/10.33271/nvngu/2021-3/064.
[26] T. Abadi, L. Le Pen, A. Zervos, W. Powrie, Improving the performance of railway tracks through ballast interventions, Proc. Inst. Mech. Eng. Part F J. Rail Rapid. Transit. 232 (2018), https://doi.org/10.1177/0954409716671545.
[27] D. Ionescu, Evaluation of the engineering behaviour of railway ballast, Civ. Min. Environ. Eng. Ph.D. (2004).
[28] Plasser&Theruer, Tamping machines, (2021). <https://www.plassertheurer.com/de/maschinen-systeme/stopfung.html> (accessed July 20, 2021).
[29] Matisa, Plain line tampers and universal tampers, (2021). <http://matisa.ch/en/matisa-products.php> (accessed July 20, 2021).
[30] Tulazheldormash, Straightening and tamping finishing technology, (2021). <http://centr.prom-rus.com/cat-transport/jeleznodorojnii-transport-zapchasti/16177> (accessed July 20, 2021).
[31] A. Atamanyuk, Technology of Ballast Layer Compaction by Machines of Type VPO in the Process of Deep Ballast Cleaning (in Russian), St. Petersburg State Transport University, 2010.
[32] M. Sol-Sánchez, F. Moreno-Navarro, M.C. Rubio-Gámez, Analysis of ballast tamping and stone-blowing processes on railway track behaviour: the influence of using USPs, Geotechnique 66 (2016), https://doi.org/10.1680/jgeot.15.P.129.
[33] M. Audley, J.D. Andrews, The effects of tamping on railway track geometry degradation, Proc. Inst. Mech. Eng. Part F J. Rail Rapid Transit. 227 (2013), https://doi.org/10.1177/0954409713480439.
[34] B. Aursudkij, A Laboratory Study of Railway Ballast Behaviour under Traffic Loading and Tamping Maintenance, University of Nottingham, 2007.
[35] I. Soleimanmeigouni, A. Ahmadi, I.A. Khouy, C. Letot, Evaluation of the effect of tamping on the track geometry condition: a case study, Proc. Inst. Mech. Eng. Part F J. Rail Rapid Transit. 232 (2018), https://doi.org/10.1177/0954409716671548.
[36] S. Aingaran, L. Le Pen, A. Zervos, W. Powrie, Modelling the effects of trafficking and tamping on scaled railway ballast in triaxial tests, Transp. Geotech. 15 (2018), https://doi.org/10.1016/j.trgeo.2018.04.004.
[37] D. Kurhan, M. Havrylov, The Mathematical Support of Machine Surfacing for the Railway Track, Acta Tech. Jaurinensis. 13 (2020), https://doi.org/10.14513/actatechjaur.v13.n3.556.
[38] C. Esveld, Modern Railway Track, MRT Production, Zaltbommel, 2014.

[39] N. Pfaff, Comparison of spatial and local tamping technologies (in German), TU Dresden, 2018. <https://tu-dresden.de/bu/verkehr/ibv/gvb/die-professur/termine/20180703_DA_Pfaff>.
[40] D.S. Kim, S.H. Hwang, A. Kono, T. Matsushima, Evaluation of ballast compactness during the tamping process by using an image-based 3D discrete element method, Proc. Inst. Mech. Eng. Part F J. Rail Rapid Transit. 232 (2018), https://doi.org/10.1177/0954409718754927.
[41] X.J. Wang, B. Hua, B. Hu, Y.L. Chi, Y.F. Ding, The research on the DEM simulation of the railway ballast tamping process, Adv. Mater. Res. (2013), https://doi.org/10.4028/www.scientific.net/AMR.724-725.1723.
[42] X. Wang, Y. Chi, W. Li, T. Zhou, Study on the DEM simulation of the granular railway ballast bed tamping, Adv. Mater. Res. (2012), https://doi.org/10.4028/www.scientific.net/AMR.524-527.3256.
[43] W. Hou, B. Feng, W. Li, E. Tutumluer, Evaluation of ballast behavior under different tie support conditions using discrete element modeling, Transp. Res. Rec. 2672 (2018), https://doi.org/10.1177/0361198118790643.
[44] W.L. Lim, G.R. McDowell, Discrete element modelling of railway ballast, Granul. Matter. 7 (2005) 19–29.
[45] E. Tutumluer, Y. Qian, Y.M.A. Hashash, J. Ghaboussi, D.D. Davis, Discrete element modelling of ballasted track deformation behaviour, Int. J. Rail Transp. 1 (2013), https://doi.org/10.1080/23248378.2013.788361.
[46] B. Indraratna, N.T. Ngo, C. Rujikiatkamjorn, J.S. Vinod, Behavior of fresh and fouled railway ballast subjected to direct shear testing: discrete element simulation, Int. J. Geomech. 14 (2014), https://doi.org/10.1061/(asce)gm.1943-5622.0000264.
[47] E. Juhasz, R.M. Movahedi, I. Fekete, S. Fischer, Discrete element modelling of particle degardation of railway ballast material with PFC3D Software, Sci. Transp. Progress. Bull. Dnipropetr. Natl. Univ. Railw. Transp. (2019). https://doi.org/10.15802/stp2019/194472.
[48] Á. Orosz, P.T. Zwierczyk, Analysis of the stress state of a railway sleeper using coupled fem-dem simulation, in, Proc. - Eur. Counc. Model. Simulation, ECMS (2020), https://doi.org/10.7148/2020-0261.
[49] B. Suhr, K. Six, Simple particle shapes for DEM simulations of railway ballast: influence of shape descriptors on packing behaviour, Granul. Matter. 22 (2020), https://doi.org/10.1007/s10035-020-1009-0.
[50] D. Nishiura, H. Sakai, A. Aikawa, S. Tsuzuki, H. Sakaguchi, Novel discrete element modeling coupled with finite element method for investigating ballasted railway track dynamics, Comput. Geotech. 96 (2018), https://doi.org/10.1016/j.compgeo.2017.10.011.
[51] Y. Guo, V. Markine, G. Jing, Review of ballast track tamping: mechanism, challenges and solutions, Constr. Build. Mater. 300 (2021), 123940.
[52] H. Huang, Discrete Element Modeling of Railroad Ballast using Imaging Based Aggregate Morphology Characterization, University of Illinois, 2010.
[53] E. Tutumluer, H. Huang, Y. Hashash, J. Ghaboussi, Aggregate Shape Effects on Ballast Tamping and Railroad Track Lateral Stability, AREMA Annu. Conf. (2006).
[54] S. Shi, L. Gao, X. Cai, H. Yin, X. Wang, Effect of tamping operation on mechanical qualities of ballast bed based on DEM-MBD coupling method, Comput. Geotech. 124 (2020), https://doi.org/10.1016/j.compgeo.2020.103574.
[55] C. Pereira Silva, M.S. Dersch, J.R. Edwards, Quantification of the effect of train type on concrete sleeper ballast pressure using a support condition back-calculator, Front. Built Environ. 6 (2020), https://doi.org/10.3389/fbuil.2020.604180.
[56] D. Kurhan, M. Kurhan, Modeling the Dynamic Response of Railway Track, in: IOP Conf. Ser. Mater. Sci. Eng., 2019, https://doi.org/10.1088/1757-899X/708/1/012013.
[57] M. Sysyn, V. Kovalchuk, U. Gerber, O. Nabochenko, B. Parneta, Laboratory evaluation of railway ballast consolidation by the non-destructive testing, Commun. - Sci. Lett. Univ. Zilina. 21 (2019), https://doi.org/10.26552/com.c.2019.2.81-88.
[58] T. Dahm, Grundlagen der Geophysik, Lect. Notes. (2015).
[59] MathWorks, MATLAB R2020b, (2020). <https://www.mathworks.com/products/new_products/release2020b.html> (accessed July 20, 2021).
[60] J. Liu, G. Liu, T. Gao, P. Wang, J. Xiao, C. Hu, Settlement and Stress Distribution Characteristics of a Railway Ballast Layer under a Dynamic Load, 2021.
[61] Y. Guo, C. Zhao, V. Markine, C. Shi, G. Jing, W. Zhai, Discrete element modelling of railway ballast performance considering particle shape and rolling resistance, Railw. Eng. Sci. 28 (2020), https://doi.org/10.1007/s40534-020-00216-9.
[62] C.M. Wensrich, A. Katterfeld, Rolling friction as a technique for modelling particle shape in DEM, Powder Technol. 217 (2012), https://doi.org/10.1016/j.powtec.2011.10.057.
[63] M. Sysyn, O. Nabochenko, V. Kovalchuk, S. Przybyłowicz Michałand Fischer, Investigation of interlocking effect of crushed stone ballast during dynamic loading, Reports, Mech. Eng. 2 (2021) 65–76.
[64] C. Tuschl, B. Oswald-tranta, S. Eck, Inductive thermography as non-destructive testing for railway rails, Appl. Sci. 11 (2021), https://doi.org/10.3390/app11031003.
[65] M. Gupta, M.A. Khan, Advances in applications of non-destructive testing (NDT): a review, Int. Res. J. Eng. IT Sci. Res. 7 (2021), https://doi.org/10.21744/irjeis.v7n3.1003.
[66] J. Kanis, V. Zitrický, V. Hebelka, P. Lukáč, M. Kubín, Innovative diagnostics of the railway track superstructure, Transp. Res. Procedia (2021), https://doi.org/10.1016/j.trpro.2021.02.017.
[67] R. De Bold, Non-destructive Evaluation of Railway Trackbed Ballast, University of Edinburgh, 2011.
[68] M. Sysyn, O. Nabochenko, V. Kovalchuk, U. Gerber, Evaluation of railway ballast layer consolidation after maintenance works, Acta Polytech. 59 (2019), https://doi.org/10.14311/AP.2019.59.0077.
[69] T. Gras, M.A. Hamdi, M. Ben Tahar, O. Tanneau, L. Beaubatie, On a coupling between the Finite Element (FE) and the Wave Finite Element (WFE) method to study the effect of a local heterogeneity within a railway track, J. Sound Vib. 429 (2018), https://doi.org/10.1016/j.jsv.2018.05.011.
[70] X. Bian, W. Li, J. Hu, H. Liu, X. Duan, Y. Chen, Geodynamics of high-speed railway, Transp. Geotech. 17 (2018), https://doi.org/10.1016/j.trgeo.2018.09.007.
[71] A. Romero, P. Galvín, J. Domínguez, 3D non-linear time domain FEM-BEM approach to soil-structure interaction problems, Eng. Anal. Bound. Elem. 37 (2013), https://doi.org/10.1016/j.enganabound.2013.01.001.
[72] I.O. Bondarenko, D.M. Kurgan, Solution of the problems of system reliability by modeling the stress-strain state of rail track using the theory of elastic waves propagation, Sci. Transp. Progress. Bull. Dnipropetr. Natl. Univ. Railw. Transp. (2013), https://doi.org/10.15802/stp2013/9608.